Beyond the random phase approximation with a local exchange vertex

Maria Hellgren, Nicola Colonna, Stefano de Gironcoli

▶ To cite this version:

HAL Id: hal-01936969
https://hal.science/hal-01936969

Beyond the random phase approximation with a local exchange vertex

Maria Hellgren,[1] Nicola Colonna,[2] and Stefano de Gironcoli[3, 4]

[1]*Sorbonne Université, Muséum National d'Histoire Naturelle,*
UMR CNRS 7590, IRD, Institut de Minéralogie,
de Physique des Matériaux et de Cosmochimie, IMPMC, 4 place Jussieu, 75005 Paris, France
[2]*Theory and Simulation of Materials (THEOS), École Polytechnique Federale de Lausanne, 1015 Lausanne, Switzerland*
[3]*International School for Advanced Studies (SISSA), Via Bonomea 265, I-34136 Trieste, Italy*
[4]*CRS Democritos, CNR-IOM Democritos, Via Bonomea 265, I-34136 Trieste, Italy*
(Dated: November 27, 2018)

With the aim of constructing an electronic structure approach that systematically goes beyond the GW and random phase approximation (RPA) we introduce a vertex correction based on the exact-exchange (EXX) potential of time-dependent density functional theory. The EXX vertex function is constrained to be local but is expected to capture similar physics as the Hartree-Fock vertex. With the EXX vertex we then unify different beyond-RPA approaches such as the various re-summations of RPA with exchange (RPAx) and the second order screened exchange (SOSEX) approximation. The theoretical analysis is supported by numerical studies on the hydrogen dimer and the electron gas, and we discuss the role of including the vertex correction in both the screened interaction and the self energy. Finally, we give details on our implementation within the plane-wave pseudo potential framework and demonstrate the excellent performance of the different RPAx methods in describing the energetics of hydrogen and van der Waals bonds.

I. INTRODUCTION

Kohn-Sham (KS) density functional theory (DFT)[1,2] has been extremely successful in predicting structural and vibrational properties of a wide range of systems. However, for sparse systems, or systems in reduced dimensions, the standard local or semi-local approximations are unreliable and sometimes fail qualitatively. Examples are the various silica polymorphs which require a proper description of the van der Waals forces,[3,4] or the layered materials which often exhibit effects of strong electron correlation.[5] Moreover, in reduced dimensions, excitonic effects become increasingly important and may be strong enough to influence ground-state properties.[6]

Although highly accurate methods such as coupled cluster or quantum Monte Carlo (QMC) could overcome these limitations high computational cost limits them to the study of very selected systems. A cheaper solution to at least some of the problems is to include a fraction of Hartree-Fock (HF) exchange via the so-called hybrid functionals.[7,8] These functionals are well-known to improve the electronic structure of, e.g., transition metal compounds.[9] On the other hand, the hybrid functionals miss the van der Waals forces and rely on a parametrisation which often turns out to be system dependent.

Another route is to use many-body perturbation theory (MBPT) based on Green's functions which is a complete theoretical framework for studying both ground and excited state properties. A popular approximation to the many-body self-energy Σ is the GW approximation[10] (GWA) which simultaneously captures the exchange interaction and the van der Waals forces.[11,12] The GWA is widely used for band-structure calculations (i.e. quasiparticle energies) and total energy calculations are becoming feasible, at least within the random phase approximation (RPA), which can be seen as the variation-ally best GW total energy within a restricted space of KS Green's functions.[13–15] Approximations beyond the GW self-energy can be constructed using diagrammatic techniques by, for example, including the second order screened exchange (SOSEX) diagram.[16–20] Since, in general, it is not obvious which set of diagrams to include different approximation schemes have been developed. In the so-called Φ/Ψ-derivable schemes[21] diagrams are chosen such that only conserving approximations are generated, i.e., approximations that conserve energy, momentum and particle number.[22,23] Another approach is Hedin's iterative procedure, in which approximations are generated from a vertex function $\Gamma = 1 + \delta\Sigma/\delta V$ where $\Sigma = iGW\Gamma$ and V is the single particle potential.[10] By, e.g., starting from GW (i.e. $\Gamma = 1$) the self-energy can be updated iteratively. It is also possible to start from a simpler approximation to the self-energy, such as the HF approximation, generating a non-local vertex function similar to the one used in the Bethe-Salpeter equation.

In this work we study an approximate local HF vertex derived from the exact-exchange (EXX) potential of time-dependent density functional theory (TDDFT). The EXX potential is obtained by minimizing the HF energy in a constrained space of local potentials.[24] Local vertex corrections derived from LDA and GGA's have been studied in the context of quasi-particle energies, but their effect on the GW gaps was quite small.[25–27] The HF or the local EXX vertex should more accurately capture the electron-hole interaction, expected to be important for correcting the deficiencies found within the self-consistent GWA.[28] The main focus of this paper will be on the total energy and we will show how one can consistently generate different approximations beyond the RPA total energy using the EXX vertex. In this way, we establish theoretical connections between the different variants

of RPA with exchange (RPAx), usually defined in terms of the density response function,[29–39] as well as between the RPAx and the SOSEX total energy approximation. The analysis also provides a many-body perspective on approximations usually defined within DFT.

The paper is organized as follows. In Sec. II we derive the basic equations for the adiabatic connection total energy formula within MBPT and DFT. We then define the vertex function, which establishes a connection between the two frameworks. We also review the comparison between GW and RPA. In Sec. III we define the local HF or EXX vertex and use it to derive previously defined approximations based on RPAx and a slightly new variant of SOSEX. In Sec. IV we present numerical results on H_2 and the electron gas to support the theoretical discussion in Sec. III. We also present results on the A24 test-set[40] to demonstrate the performance of the different RPAx methods in describing hydrogen and van der Waals bonds. In the end, we present numerical details from our implementation within the plane-wave and pseudo potential framework. Finally, in Sec. V, we present our conclusions.

II. CORRELATION ENERGY

We start by deriving the exact adiabatic connection formula for the correlation energy in terms of the single-particle Green's function G. Similar derivations can be found in Refs. 41 and 42.

The Hamiltonian of the interacting electronic system is given by

$$\hat{H} = \hat{T} + \hat{V}_{\text{ext}} + \hat{W} \qquad (1)$$

where $\hat{T}$ is the kinetic energy operator, $\hat{V}_{\text{ext}}$ is the external nuclear potential and $\hat{W}$ is Coulomb interaction between the electrons. The adiabatic connection path is defined in terms of a parameter $\lambda \in [0,1]$ that linearly scales the Coulomb interaction $\hat{W}$ from zero to full interaction strength. A single-particle potential V^λ is added to the Hamiltonian such that the density is kept fixed to its interacting value ($\lambda = 1$) at every value of λ. Introducing the Hartree (H) and exchange-correlation (xc) potential $\hat{V}_{\text{Hxc}}$, as defined within KS DFT, we thus write the scaled Hamiltonian on the adiabatic connection path as follows

$$\hat{H}^\lambda = \hat{T} + \hat{V}_{\text{ext}} + \hat{V}_{\text{Hxc}} - \hat{V}^\lambda + \lambda\hat{W} \qquad (2)$$

where

$$\hat{V}^{\lambda=1} = \hat{V}_{\text{Hxc}}, \quad \hat{V}^{\lambda=0} = 0. \qquad (3)$$

With the Hamiltonian defined in Eq. (2) we derive the corresponding single-particle Green's function and write it in terms of a Dyson equation

$$G_\lambda = G_s + G_s[\Sigma_\lambda[G_\lambda] - V^\lambda]G_\lambda \qquad (4)$$

where Σ_λ is the irreducible self-energy and G_s is the Green's function of the $\lambda = 0$ system (i.e. the KS Green's function). Using standard tricks[41] we can write the total energy at full interaction strength as an integral over the coupling constant λ. Defining the single-particle energy

$$E_s = T_s + \int n v_{\text{ext}} + E_{\text{H}} \qquad (5)$$

the total energy is written as

$$E = E_s - \frac{i}{2}\int\frac{d\omega}{2\pi}\int\frac{d\lambda}{\lambda}\text{Tr}\{\Sigma_\lambda[G_\lambda]G_\lambda\} \qquad (6)$$

where the trace is defined as $\text{Tr}\{AB\} = \int d\mathbf{r}d\mathbf{r}' A(\mathbf{r},\mathbf{r}')B(\mathbf{r}',\mathbf{r})$ and the convergence factor ($e^{i\omega\eta}$) has been suppressed. This is an exact formula from which one can generate approximate total energies from any approximate Σ.

An alternative way to write the correlation energy is in terms of the density correlation function (or the reducible polarization propagator) χ

$$E = E_s + \frac{i}{2}\int\frac{d\omega}{2\pi}\int d\lambda\,\text{Tr}\{v[\chi_\lambda - \delta n]\} \qquad (7)$$

where $\delta n = \delta(\mathbf{r},\mathbf{r}')n(\mathbf{r})$. In this form, approximations are generated diagrammatically via the Bethe-Salpeter equation, or via the linear response TDDFT Dyson equation.

In order to connect the two expressions, Eq. (6) and Eq. (7), we define the irreducible polarization propagator P in terms of the vertex function Γ

$$P = -iGG\Gamma, \quad \Gamma = -\frac{\delta G^{-1}}{\delta V} = 1 + \frac{\delta\Sigma}{\delta V} \qquad (8)$$

where $V = v_{\text{ext}} + v_{\text{H}}$. With these quantities it is possible to rewrite the scaled density correlation function using the relation

$$\chi_\lambda v = \frac{1}{\lambda}P_\lambda W_\lambda \qquad (9)$$

in which $W = v + vPW$ is the screened Coulomb interaction. Since P is given by Eq. (8) and $\Sigma = iGW\Gamma$ we can rewrite Eq. (7) in the form of Eq. (6).

Within TDDFT the density correlation function is determined from the time-dependent KS system which is defined to reproduce the exact interacting density with a time-dependent local single-particle potential.[43] The TDDFT Dyson equation reads

$$\chi_\lambda = \chi_s + \chi_s[\lambda v + f_{\text{xc}}^\lambda]\chi_\lambda \qquad (10)$$

where $\chi_s = -iG_sG_s$ is the KS polarization propagator and f_{xc}^λ is the functional derivative of the time-dependent xc potential with respect to the density. The irreducible polarization propagator P is then determined from $P = \chi_s + \chi_s f_{\text{xc}} P$. But, this expression can easily be rearranged to $P = -iG_sG_s\Gamma_{\text{xc}}$, that is, in terms of a local vertex function defined as

$$\Gamma_{\text{xc}} = 1 + \frac{\delta v_{\text{xc}}}{\delta V}. \qquad (11)$$

In this way we can rewrite Eqs. (7) as

$$E = E_s - \frac{i}{2} \int \frac{d\omega}{2\pi} \int \frac{d\lambda}{\lambda} \text{Tr}\{\Sigma_\lambda^{GW\Gamma_{\text{xc}}} G_s\} \qquad (12)$$

where $\Sigma^{GW\Gamma_{\text{xc}}} = iG_s W\Gamma_{\text{xc}}$, which can be compared to Eq. (6). Notice that if the exact xc kernel is used this is an exact expression for the correlation energy. This, however, does not mean that $\Sigma^{GW\Gamma_{\text{xc}}}$ is the exact self-energy which should be defined in terms of the fully non-local vertex function. The extent to which a local vertex can approximate the exact vertex was studied in Ref. 27 and 44.

A. RPA and GW

The GWA and RPA have already been thoroughly compared[45,46] but for the sake of completeness we review this comparison here. Within the GWA we can calculate the total energy via Eq. (6) by simply setting

$$\Sigma_\lambda^{\text{GW}} = iG_\lambda W_\lambda, \quad W_\lambda = \lambda v + \lambda v P_0 W_\lambda. \qquad (13)$$

The screened interaction is calculated in the time-dependent Hartree approximation (or RPA) for which $P_0 = -iGG$.

The RPA for the total energy is given by

$$E^{\text{RPA}} = E_s + \frac{i}{2} \int \frac{d\omega}{2\pi} \int d\lambda \text{Tr}\{v[\chi_\lambda^{\text{RPA}} - \delta n]\} \qquad (14)$$

where

$$\chi_\lambda^{\text{RPA}} = \chi_s + \lambda \chi_s v \chi_\lambda^{\text{RPA}}. \qquad (15)$$

Following the steps in the previous section [Eqs. (8)-(12)] we see that this response function corresponds to $\Gamma_{\text{xc}} = 1$. We can thus write

$$E^{\text{RPA}} = E_s - \frac{i}{2} \int \frac{d\omega}{2\pi} \int \frac{d\lambda}{\lambda} \text{Tr}\{\Sigma_\lambda^{\text{GW}}[G_s] G_s\} \qquad (16)$$

and we see that this exactly corresponds to Eq. (6) in the GWA but with G_λ replaced by G_s. We notice that the diagrammatic structure within the GWA is preserved in the RPA. Furthermore, since only the explicit λ-dependence is retained, the λ-integral is easily carried out leading to the following expression

$$E^{\text{RPA}} = E_s - \frac{i}{2} \int \frac{d\omega}{2\pi} \text{Tr}\{\ln[1 + ivG_s G_s]\}. \qquad (17)$$

Since the GW self-energy is Φ-derivable, meaning that the self-energy can be generated from a functional $\Phi[G]$, i.e., $\Sigma = \delta\Phi[G]/\delta G$, also the λ integral in Eq. (6) can be performed analytically. This leads to a total energy of the form

$$E^{\text{GW}} = -\frac{i}{2} \int \frac{d\omega}{2\pi} \text{Tr}\{\ln[1 + ivGG]\} + E_{\text{H}}$$
$$+ i \int \frac{d\omega}{2\pi} \text{Tr}\left[GG_s^{-1} - 1 + \ln(-G^{-1})\right]. (18)$$
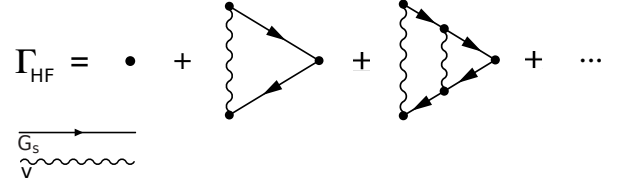

Figure 1. Diagrammatic expansion of the exchange vertex in the HF approximation. Wiggly lines correspond to the bare Coulomb interaction v.

This is a functional of G (also known as the Klein functional) which is stationary when G obeys the Dyson equation. If we replace G with G_s it is easy to show that this expression is equivalent to Eq. (17). We thus have a second way to compare the GWA and RPA.[45,46] The RPA is the GW Klein energy constrained to the space of KS Green's functions.

III. LOCAL HARTREE-FOCK VERTEX

We will now improve the GWA and RPA by constructing an approximate vertex function (Eq. (8)) from the HF self-energy ($\Sigma_{\text{HF}} = iGv$)

$$\Gamma_{\text{HF}} = 1 + \frac{\delta\Sigma_{\text{HF}}}{\delta V}. \qquad (19)$$

We note that since the self-energy depends on two arguments the vertex depends on three arguments (three space and time variables). The diagrammatic expansion of the HF vertex is given in Fig. 1. From the diagrammatic structure it is easy to see that the electron-hole interaction is accounted for. If we replace the bare Coulomb interaction with a statically screened Coulomb interaction this vertex generates what is usually referred to as the Bethe-Salpeter equation for the polarization propagator.

An approximate local HF vertex can be defined in terms of the local time-dependent exact-exchange (EXX) potential v_{x}

$$\Gamma_{\text{x}} = 1 + \frac{\delta v_{\text{x}}}{\delta V} = \frac{1}{1 - \Gamma_{\text{x}}^1} \qquad (20)$$

where

$$\Gamma_{\text{x}}^1 = \frac{\delta v_{\text{x}}}{\delta V_s}, \quad V_s = v_{\text{ext}} + v_{\text{Hx}}. \qquad (21)$$

Since the local approximation $v_{\text{x}} \sim \Sigma_{\text{HF}}$ depends only on one argument the corresponding local vertex function Γ_{x} has only two arguments as opposed to three. The time-dependent EXX potential is determined by the linearized Sham-Schlüter equation[47] and has been studied in several previous work. It can, e.g., be shown that v_{x} exactly reproduce the HF density to first order in the Coulomb interaction. The equation for Γ_{x}^1 is illustrated diagrammatically in Fig. 2. We note that the local EXX vertex

reproduce the response function of the full HF vertex to first order in the Coulomb interaction.[48]

Using the chain rule Eq. (21) also defines the standard EXX kernel

$$f_{\mathrm{x}} = \frac{\delta v_{\mathrm{x}}}{\delta n} = \Gamma_{\mathrm{x}}^1 \chi_s^{-1}. \qquad (22)$$

With the EXX kernel we can generate the TDDFT density correlation function which is usually referred to as the RPAx response function

$$\chi^{\mathrm{RPAx}} = \chi_s + \chi_s[v + f_{\mathrm{x}}]\chi^{\mathrm{RPAx}}. \qquad (23)$$

This response function has been applied to atoms and molecules as well as to silicon for the calculation of excitons.[30,32,48,49] Although some excitation energies are sensitive to the local approximation[30] integrated quantities such as polarizabilities and van der Waals coefficients give results similar to the nonlocal time-dependent HF (TDHF) approach.[32] In the following we will use the EXX vertex to generate a set of approximations to the total energy.

A. $\mathbf{GW\Gamma_x}$ and $\mathbf{GW\Gamma_{HF}^1}$

If we use the RPAx response function defined in Eq. (23) and insert it into the total energy of Eq. (7) we find what we have previously called the RPAx for the total energy

$$E^{\mathrm{RPAx}} = E_s + \frac{i}{2} \int \frac{d\omega}{2\pi} \int d\lambda \mathrm{Tr}\{v[\chi_\lambda^{\mathrm{RPAx}} - \delta n]\}. \qquad (24)$$

With the definition of the EXX vertex in Eq. (20) we can follow the same steps that lead to Eq. (12) and rewrite Eq. (24) as

$$E^{\mathrm{RPAx}} = E_s - \frac{i}{2} \int \frac{d\omega}{2\pi} \int \frac{d\lambda}{\lambda} \mathrm{Tr}\{\Sigma_\lambda^{GW\Gamma_{\mathrm{x}}} G_s\} \qquad (25)$$

with $\Sigma^{GW\Gamma_{\mathrm{x}}} = iG_s W\Gamma_{\mathrm{x}}$. Since the vertex is local this self-energy is approximate but is expected to mimic the self-energy with the full HF vertex. If the latter is used, the approximation to the correlation energy corresponds to the RPAx defined in Ref. 29, i.e., the correlation energy with the TDHF response function. Comparing the
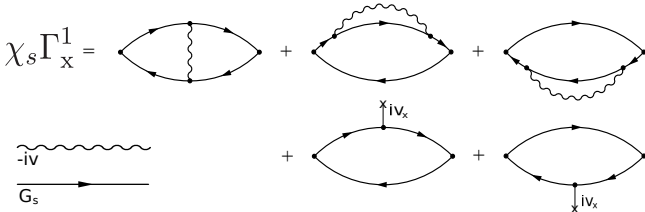

Figure 2. Equation to obtain the first order local exchange vertex Γ_{x}^1.

results of Refs. 29 and 50 to those of Ref. 51 we see similar trends. Only in the case of the Be dimer there is a qualitative difference and it is found that the use of a nonlocal potential for generating G_s strongly improves the results. We notice that neither the HF nor the EXX vertex produces Φ-derivable self-energies due to the lack of symmetry.

If we expand the EXX vertex to first order only (Γ_{x}^1) all terms in the expansion of the correlation energy have a diagrammatic representation. We can therefore write the total energy of the Γ_{x}^1-approximation [RPAx(1)] in terms of the full HF vertex to first order (Γ_{HF}^1) plus a self-energy correction

$$E^{\mathrm{RPAx}(1)} = E_s - \frac{i}{2} \int \frac{d\omega}{2\pi} \int \frac{d\lambda}{\lambda} \mathrm{Tr}\{\Sigma_\lambda^{GW\Gamma_{\mathrm{HF}}^1}[G_s]G_s\} + E_{\Sigma_s}. \qquad (26)$$

The diagrammatic representation of the first correlation term is given in Fig. 3(a). The second, self-energy correction, is of the form

$$E_{\Sigma_s} = -\frac{i}{2} \int \frac{d\omega}{2\pi} \int d\lambda \, \mathrm{Tr}\{G_s W^\lambda G^1 + G^1 W^\lambda G_s\} \qquad (27)$$

with

$$G^1 = G_s[\Sigma_{\mathrm{HF}} - v_{\mathrm{x}}]G_s. \qquad (28)$$

One of the terms in Eq. (27) is illustrated in Fig. 3(c).

Alternatively we can write the correlation energy of Eq. (26) as in Eq. (7), in terms of an approximate density correlation function obtained by expanding the irreducible polarizability to first order

$$\chi_\lambda^{\mathrm{RPAx}(1)} = P_\lambda^1 + \lambda P_\lambda^1 v \chi_\lambda^{\mathrm{RPAx}(1)}$$
$$\Rightarrow \chi_\lambda^{\mathrm{RPAx}(1)} = [1 - \lambda P_\lambda^1 v]^{-1} P_\lambda^1 \qquad (29)$$

where $P_\lambda^1 = \chi_s + \lambda \chi_s \Gamma_{\mathrm{x}}^1 = \chi_s + \lambda \chi_s f_{\mathrm{x}} \chi_s$. This approximation was studied previously for the electron gas in Ref. 35 and for the total energy of molecules in Ref. 51. By keeping the vertex to first order only cured certain pathologies due to an unscreened Coulomb interaction. We note here that in Refs. 35 and 51 we employed an additional alternative re-summation for χ based on the first order exchange kernel, called t'RPAx, which is similar to the one proposed in Ref. 34. This approximation has been shown to produce results of similar quality as RPAx(1), but since it does not have a counterpart in MBPT we will not study this approximation here.

B. SOSEX

In the RPAx(1) approximation defined above the vertex is treated to first order in both screened interaction and in the self-energy. If we set the vertex to one in the screened interaction (i.e. keeping it at the RPA level) we generate the so-called SOSEX approximation. For a

diagrammatic representation see Fig. 3(b). The total energy is given by

$$E^{\mathrm{AC-SOSEX}} =$$
$$E_s - \frac{i}{2} \int \frac{d\omega}{2\pi} \int \frac{d\lambda}{\lambda} \mathrm{Tr}\{\Sigma^{\mathrm{SOSEX}}_\lambda [G_s] G_s\} + \tilde{E}_{\Sigma_s} \quad (30)$$

where $\tilde{E}_\Sigma$ is a self-energy correction with a RPA screened interaction. This expression can also be exactly rewritten in terms of an approximate density correlation function given by

$$\chi^{\mathrm{SOSEX}}_\lambda = P^1_\lambda + \lambda \chi_s v \chi^{\mathrm{SOSEX}}_\lambda$$
$$\Rightarrow \chi^{\mathrm{SOSEX}}_\lambda = [1 - \lambda \chi_s v]^{-1} P^1_\lambda. \quad (31)$$

The SOSEX has been studied previously, both for total energies, and quasi-particle excitations of finite systems.[16–19] Total energies are obtained either from the adiabatic connection expression (Eq. (6)) or from the perturbative Galitskii-Migdal expression. It has been shown that so-called single-excitations improve the results[18] and our self-energy correction $\tilde{E}_{\Sigma_s}$ can be interpreted as an approximate single-excitation correction. In our formalism this correction naturally arises from the definition of the local EXX vertex. The so generated set of approximations RPAx, RPAx(1) and AC-SOSEX can thus be seen as a consistent way to do many-body approximations based on a local DFT framework. Self-energy corrections to the same order as the vertex naturally follows and compensate to some extent for a lack of self-consistency within the MBPT scheme. Once the EXX vertex (or the EXX kernel) is calculated all approximations follow straightforwardly (see also Appendix A). In the next section we will compare these different approximations on H_2 and the electron gas and assess their performance in describing hydrogen and van der Waals bonds.

IV. NUMERICAL RESULTS

In this section we present numerical results on H_2 and the electron gas, in order to compare the different approximations defined in the previous section, and to compare to SOSEX results obtained by other groups. We also present calculations on the A24 test-set[40] containing molecules with hydrogen and van der Waals bonds. All calculations (except for those on the electron gas) have been done with a recently released RPA/RPAx-implementation within the QUANTUM ESPRESSO package.[52] See Sec. IVC, Appendix A and Refs. 35, 53, and 54 for details regarding the implementation.

A. H_2 and the electron gas

In Fig. 4 we present H_2 dissociation curves within RPA, RPAx, RPAx(1) and AC-SOSEX, and compare the results to accurate results from Ref. 55. We also compare our AC-SOSEX to previous SOSEX results in the
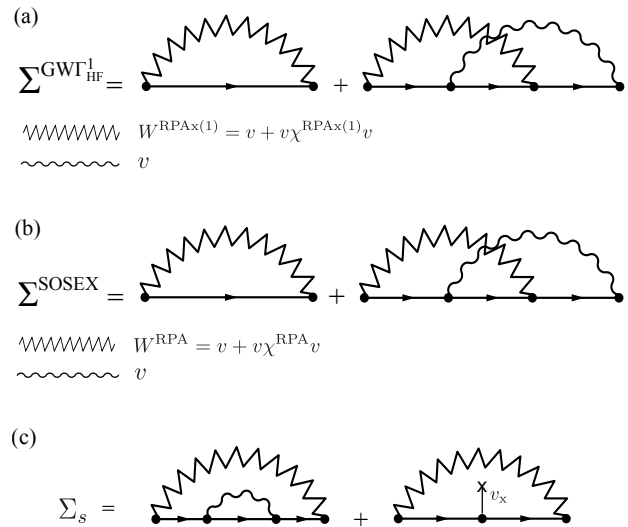

Figure 3. Diagrammatic representation of the $GW\Gamma^1_{\mathrm{HF}}$ (a) and SOSEX (b) self-energies. The self-energy correction in Eq. (27) is illustrated in (c).

literature.[56] RPA, RPAx and RPAx(1) all include the vertex correction in both the screened interaction and the self energy ($\Gamma = 1$, Γ_{x} and Γ^1_{HF} respectively). At the same time they are all able to capture the dissociation region, or static correlation, reasonably well. We note that the remaining "bump" seen in all approaches has been shown to disappear when employing a statically screened vertex.[57] Our AC-SOSEX results are essentially identical to previous results. SOSEX includes the vertex correction (Γ^1_{HF}) in the self-energy only, while it treats the screened interaction at the RPA level. This inconsistency could explain why it fails to describe dissociation into open-shell atoms.

In the dissociation limit of H_2 the one-electron H-atoms are represented as a mixture between a spin-up and a spin-down state. Such an ensemble state requires a correlated method to be described. If, instead, the H-atom is isolated it can be treated as spin-polarized and HF gives the exact non-interacting result. The RPA is based on the Hartree response and, therefore, introduces self-interaction in the correlation functional. The RPAx naturally cures this error since it is based on the full HF response.[58] It can straightforwardly be proven that also AC-SOSEX is one-electron self-interaction free (see e.g. Ref. 59). RPAx(1) will, however, contain terms to 3rd order and beyond that are non-vanishing, but expected to be small.

In Fig. 5 we present the correlation energy per particle in the homogeneous electron gas (HEG). We compare our AC-SOSEX energies to previous SOSEX results by Freeman[16] and to accurate QMC results.[60,61] Again, we find that our AC-SOSEX agrees very well with previous SOSEX results. Both coincides with QMC results at a given density (AC-SOSEX at $r_s = 6.3$ and SO-
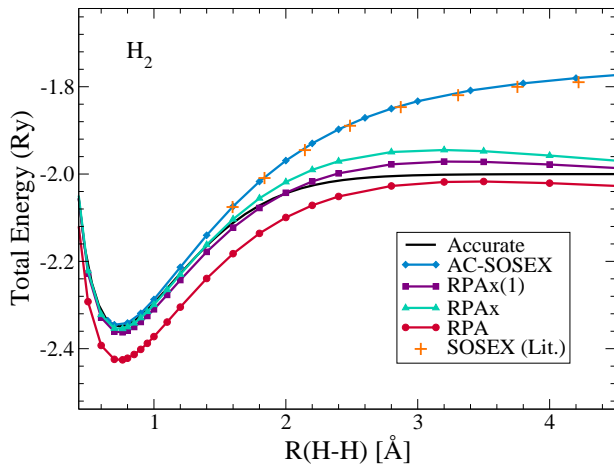
Figure 4. Dissociation curves for the hydrogen molecule within different beyond-RPA methods. Approximations derived in this work are compared to 'exact' results presented in Ref. 55 and to SOSEX results obtained by Ren *et al.* in Ref. 56
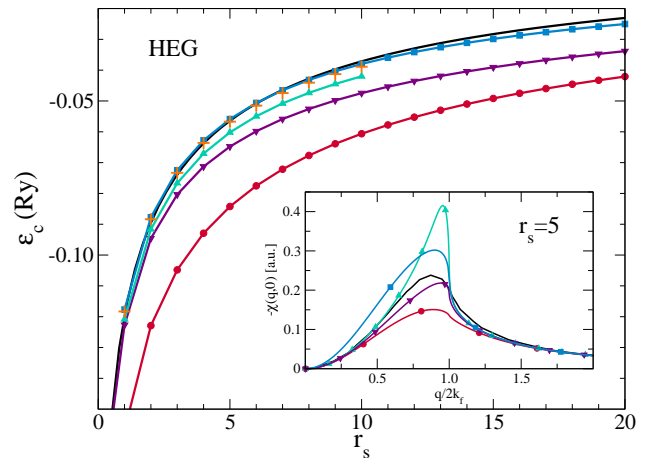
.

Figure 5. The energy per particle of the homogeneous electron gas within different beyond-RPA methods compared to QMC results of Ref. 61 and to SOSEX results of Ref. 16. Symbol and line coding as in Fig. 4. The inset shows the corresponding static response functions at $r_s = 5$.

SEX at $r_s = 4.8$). Overall, SOSEX produces energies in very good agreement with QMC even up to low densities. RPAx(1) represents a systematic improvement upon RPA, performing very well in the metallic range ($r_s < 5$) although slightly worse than RPAx. For a more detailed discussion of RPAx and RPAx(1), see Ref. 35. But, we mention here that expanding the EXX vertex to first order only, i.e. going from RPAx to RPAx(1), removes an instability of the response function at low electronic densities[35] ($r_s > 11$). A similar behavior has also been reported by the authors of Ref. 62 who observed imaginary frequencies eigenmodes for the polarization propagator computed by solving the Bethe Salpeter equation. Also in their case disregarding selected diagrams removes the instability in the low density regime.

In the inset of Fig. 5 we have plotted the static response functions at $r_s = 5$, obtained from Eq. (23), Eq. (29) and Eq. (31). Again, RPAx(1) systematically improves upon RPA and has no pathological behavior as compared to RPAx. SOSEX strongly overestimates the static response up to its maximum suggesting that the good energies are subject to effects of error cancellation.

B. Dispersion interactions: The A24 test-set

In order to test the performance of the beyond-RPA methods in describing dispersion forces we calculated the binding energies of molecular dimers in the A24 test set.[40] The results are presented in Fig. 6 and in Table 1. The RPA tends to underestimate the binding energies with a Mean Absolute Error (MAE) of 0.44 kcal/mol. SOSEX has been shown to improve the description of

dispersion interactions as compared to RPA and we find similar results in this work, with a MAE of 0.19 kcal/mol. Overall, the SOSEX energies are overestimated, in particular for the dimers with mixed bonds where the errors only slightly reduce with respect to RPA. RPAx and RPAx(1) give similar average performances (MAE of 0.14 kcal/mol and 0.13 kcal/mol, respectively) but RPAx(1) gives a more reliable improvement without exceptions.

Comparing to other beyond-RPA results in the literature we find that our approximations perform better than those of TDHF based approximations, unless a range-separation parameter is introduced.[38,50,63] As expected, our RPAx results are comparable to the RPAx results of Ref. 64.

C. Technical aspects

All molecular calculations of the ACFDT expression for the total energy were performed in a plane-wave and pseudo-potential formalism as implemented in a separate module of the QUANTUM ESPRESSO distribution.[52,65] We devote this section to review the basic aspects of our implementation of the exchange and correlation energy at all the levels of the theory discussed in Sec. II and Sec. III (for a more detailed description we refer to Refs. 35, 53, and 54). We complement the discussion with convergence tests on the relevant parameters of our implementation for a subset composed of three complexes, namely the water-ammonia, the methane-HF and the borane-methane, each one representative for a different type of bond in the A24 set.

All the ACFDT calculations have been performed in a post-DFT fashion. The KS single-particle wavefunc-
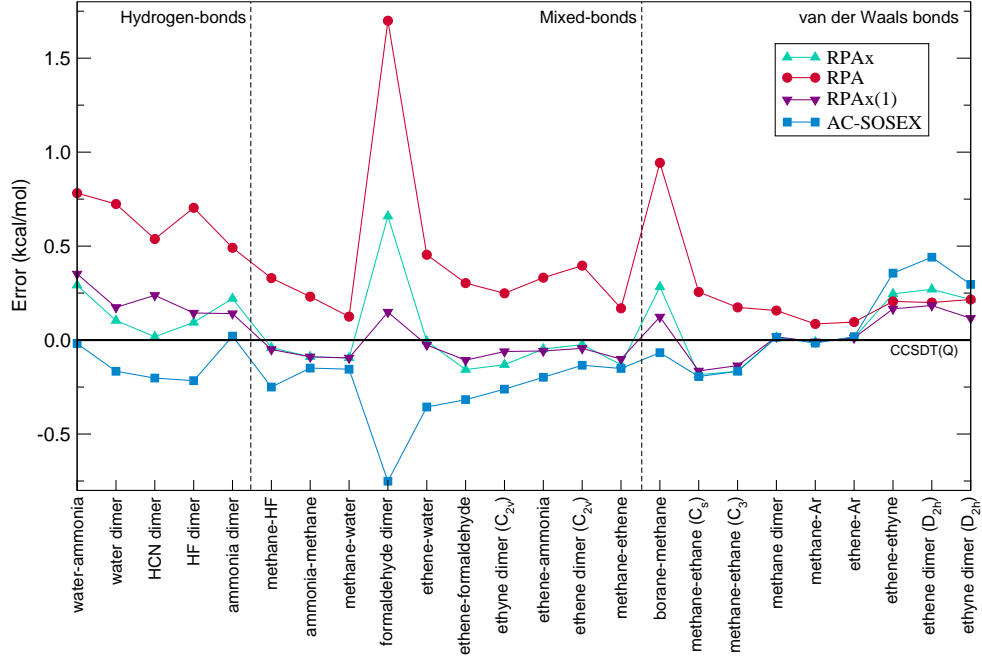
Figure 6. Error in binding energies (kcal/mol) for the molecules in the A24 test-set. Results are compared to highly accurate CCSDT(Q) results of Ref. 40. Data can be found in Table 1.

tions and energies needed as input for the ACFDT total energy calculation have been calculated at the PBE[66] level using an energy cut-off of 80 Ry; Optimized Norm-Conserving Vanderbilt (ONCV) pseudopotentials[67–69] have been used to model the electron-ion interaction. The molecules have been placed in an orthorhombic cell with 12 A of vacuum in each direction, sufficient to suppress the spurious interactions between periodic replica. As illustrated on the first and second row of Fig. 7, with this setup all the components of the binding energy (BE) converge within 0.05 kcal/mol. A slightly larger deviation is seen for the RPAx correlation BE with respects to energy cut-off (identical in all beyond-RPA methods). We note, however, that this is not due to a worse convergence with respect to the energy cut-off, but to the numerical precision associated with the EXX optimized-effective potential problem, needed for the evaluation of the RPAx correlation energy.[35] The error bars on the final beyond-RPA binding energies are estimated to be $< 3\%$ for the A24 test-set, corresponding to 0.006 kcal/mol per electron. Half of this value is estimated for the RPA binding energies.

The exact xc-energy [second term on the rhs of Eq. (7)] can be further separated into the KS EXX energy

$$E_{\mathrm{x}} = -\frac{1}{2} \int d\mathbf{r} d\mathbf{r}' \frac{|\sum_i^{\mathrm{occ}} \phi_i(\mathbf{r})\phi_i^*(\mathbf{r}')|^2}{|\mathbf{r} - \mathbf{r}'|} \qquad (32)$$

and the ACFDT correlation energy determined by the difference between the interacting and non-interacting KS response functions

$$E_{\mathrm{c}} = -\int_0^1 d\lambda \int_0^\infty \frac{du}{2\pi} \, \mathrm{Tr} \, \{v \left[\chi_\lambda(iu) - \chi_s(iu) \right] \} . \quad (33)$$

The integrable divergence appearing in a plane-wave implementation of the EXX energy would lead to a slow convergence with respect to the size of the supercell. In this work this issue has been dealt with using the method proposed by Gygi and Baldereschi[70] plus the extrapolation scheme of Nguyen and de Gironcoli,[53] although other strategies are also possible.[71,72] For all cases analyzed, this correction scheme allows us to converge the EXX contribution to the BE within 0.05 kcal/mol with 10 A of vacuum separating the molecular replicas.

The strategy we use to solve the Dyson equation for χ_λ and efficiently compute the trace over the spatial coordinates in Eq. (33) is a generalization of the projective dielectric eigenpotential method[53,73–75] and requires the solution of a well defined generalized eigenvalue problem (GEP) involving the non-interacting response function χ_s and its first order correction in the limit of vanishing coupling-constant $\mathcal{H}_{\mathrm{Hx}} = \chi_s(v + f_{\mathrm{x}})\chi_s$. The set of eigenvectors of the GEP defines an optimal basis set on which i) the response matrices have a compact representation and ii) the Dyson equation has a straightforward solution, as detailed in Appendix A. Most importantly, only the lowest-lying eigenvectors and eigenvalues of the GEP at hand are relevant for the correlation energy calculation, and an efficient iterative diagonalization techniques can be used to compute the first N_{eig} lowest-lying eigen-
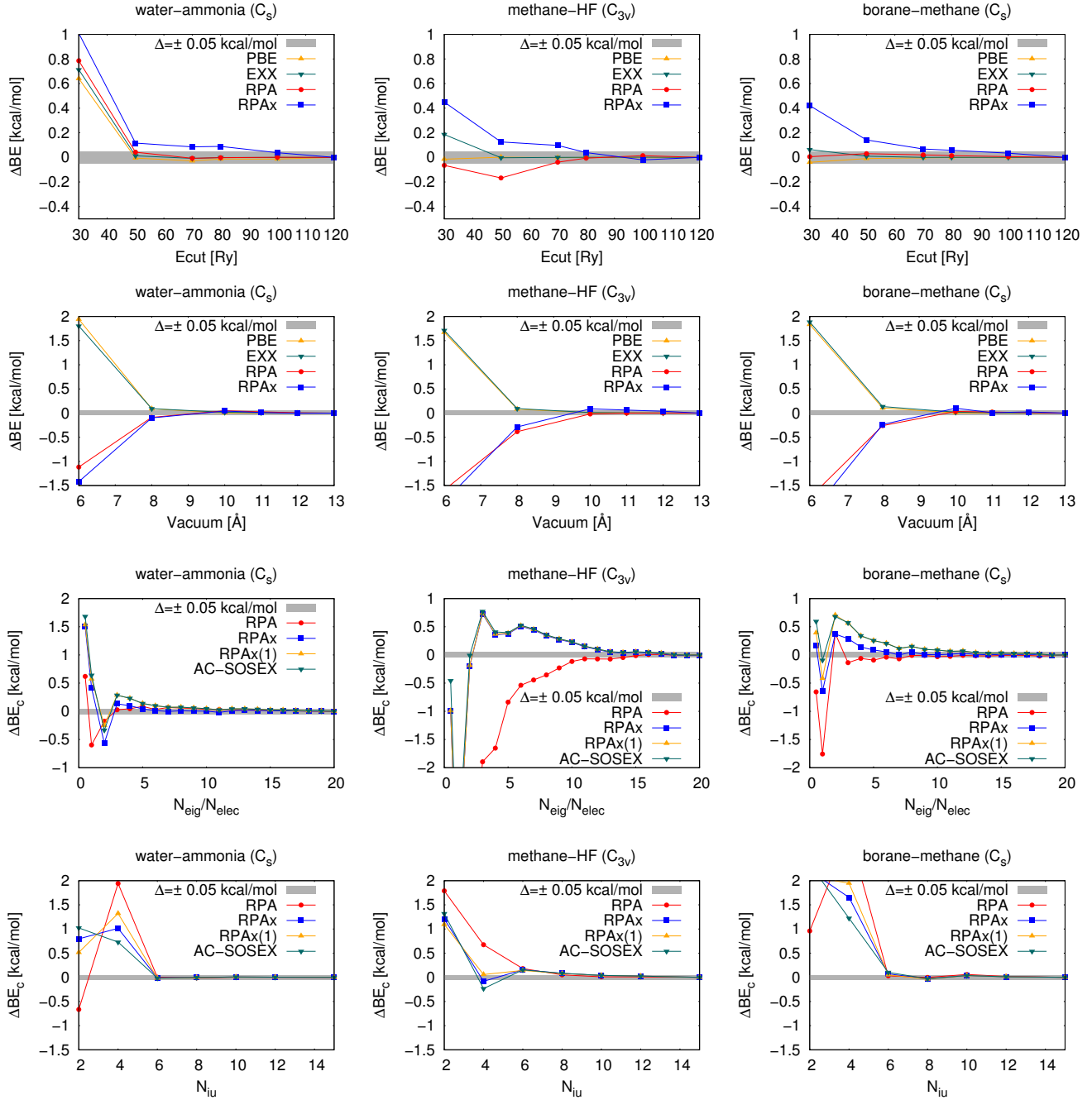
Figure 7. Convergence of the binding energy, at all levels of theory presented in the text, with respect to kinetic energy cut-off (first row), vacuum (second row), number of eigenvalues N_{eig} (third row) and number of frequencies N_{iu} (last row) for three representative molecules in the A24 test-set. In each plot and for each approximation, the zero is set by the most converged calculation.

values/eigenvectors of the problem. Moreover, the matrix elements of χ_s and of $\mathcal{H}_{\text{x}} = \chi_s f_{\text{x}} \chi_s$, needed for the solution of the GEPs, can be efficiently computed[35,53] resorting to the linear response machinery of density-functional perturbation theory[76] (DFPT) thus avoiding explicit summations over empty states.

Once the GEP is solved, the trace over spatial coordi-

nates can be written as a sum over a simple function $\mathcal{E}_c$ of the GEP eigenvalue e_α (and eventually of the diagonal matrix elements of χ_s and $\mathcal{H}_{\text{x}}$; see Appendix A for the actual expression of $\mathcal{E}_c$), and a compact expression for

the correlation energy is obtained:

$$E_{\rm c} = -\int_0^1 d\lambda \int_0^\infty \frac{du}{2\pi} \sum_{\alpha=1}^{N_{\rm eig}} \mathcal{E}_c[e_\alpha(iu,\lambda),\lambda]. \qquad (34)$$

Here the frequency integral has been moved from the real to the imaginary axis of the complex plane[77] to take advantage of the smooth behavior of the response functions for an efficient numerical quadrature (see below). The integration over the coupling constant is analytic for all the approximations but the RPAx(1) for which the eigenvalues $e_\alpha^{\rm RPAx(1)}$ inherit a non trivial dependence on the coupling constant from the λ-dependent RPAx(1) GEP (see Appendix A 3). In this case a numerical integration can be efficiently performed using a Gauss-Legendre quadrature. Usually very few points are needed to converge the integral within 0.01 kcal/mol (see Fig. 8). For all the other approximations the GEPs do not depend on λ and only the explicit dependence of $\mathcal{E}_c$ on the coupling constant has to be considered. In these cases a straightforward analytic integration is always possible.

The number of eigenvalues N_{eig} set the dimension of the optimal basis set used to represent the response functions, and, therefore, it is a convergence parameter. The third row of Fig. 7 shows the dependence of the correlation binding energy on N_{eig} for the selected subset of molecules. In all the cases and for all the approximations studied, a relatively small number of eigenvalues, never larger than 20 times the number of electrons in the system at hand, is sufficient to converge the ACFDT correlation energy contribution to the BE within 0.05 kcal/mol.

Finally, the integral over the imaginary frequency iu can be efficiently performed using a Gauss-Legendre quadrature. A standard mesh of point $z_i \in [0,\pi/2]$ is mapped on an imaginary-frequency grid between $[0,+\infty)$ using the transformation $u_i = (\varepsilon_{HL} - cz_i)\tan(z_i)$ where ε_{HL} is the DFT HOMO-LUMO gap of the systems and the parameter c is set by the upper integration limit ($u_{\max} = 200$ Ry). This transformation takes into account the typical dependence of the response functions on the imaginary frequency and the fact that at small frequency the scale of the excitation energies is given by the HOMO-LUMO gap. With this strategy a grid with $N_{\rm iu} = 10$ points is usually sufficient to converge the ACFDT energy within 0.05 kcal/mol as illustrated on the last row of Fig. 7.

V. CONCLUSIONS

In this work we have defined a local EXX vertex based on the EXX kernel of TDDFT. This allowed us to unify different beyond-RPA approaches such as the various resummations of RPAx and the SOSEX approximation, as well as to give a many-body perspective on approximations normally defined within DFT.

We have tested the theory on the H_2 molecule and the electron gas and we find that our AC-SOSEX agrees well with previous results in the literature. Although AC-SOSEX gives excellent total energies for the electron gas, it cannot be well represented as an approximation to the density response function. This could explain the poor performance in the dissociation region of H_2. On the contrary, approximations that incorporate the vertex correction in both the screened interaction and in the self-energy (RPA, RPAx and RPAx(1)) dissociate H_2 correctly.

In terms of an overall performance we find that the RPAx(1) gives the most reliable results. It is as accurate as RPAx but shows no pathologies for any of the systems studied so far. High quality results within a reasonable computational cost are obtained on the A24 test-set, paving the way for accurate *ab-initio* treatment of sparse systems.

Appendix A: The auxiliary basis sets

We provide in this section additional information on how the auxiliary basis set, used to solve the Dyson equation and calculate the trace over spatial coordinates, is computed for each approximation described in the text.

1. The RPA correlation energy

The evaluation of the RPA correlation energy is based on an eigenvalue decomposition of the noninteracting response function and has been carefully detailed in Ref. 53; we summarize here the main features of the RPA implementation because the solution of the RPA problem is a prerequisite for all the exchange-corrected approximations.

For each point on the imaginary-frequency grid the generalized eigenvalue problem (GEP)

$$v\chi_s|w_i\rangle = e_i|w_i\rangle, \qquad (A1)$$

is solved (the dependence on the imaginary frequency is implicitly assumed). Once the solution of the GEP is available the RPA Dyson equation, Eq. (16), can be readily solved since $\{w_i\}$ are also eigenvectors of $v\chi_\lambda^{\rm RPA}$ with eigenvalues $e_i^{\rm RPA} = e_i/(1 - \lambda e_i)$. The trace over spatial coordinates appearing in the expression for the

Table I. Binding energies (in kcal/mol) for the A24 test-set as obtained with the RPA, RPAx, RPAx(1) and AC-SOSEX methods Compared with CCSDT(Q) reference values[40]

		Symm	RPA	RPAx	RPAx(1)	AC-SOSEX	CCSDT(Q)
	Hydrogen-bonded systems						
01	water-ammonia	C_s	-5.71	-6.20	-6.14	-6.51	-6.492
02	water dimer	C_s	-4.27	-4.89	-4.82	-5.16	-4.994
03	HCN dimer	C_s	-4.20	-4.72	-4.50	-4.94	-4.738
04	HF dimer	C_s	-3.86	-4.47	-4.42	-4.78	-4.564
05	ammonia dimer	C_{2h}	-2.65	-2.92	-3.00	-3.12	-3.141
	ME		0.64	0.14	0.21	-0.12	—
	MAE		0.64	0.14	0.21	0.13	—
	MA%E		13.8%	3.2%	4.3%	2.7%	—
	Mixed-type systems						
06	methane-HF	C_{3v}	-1.33	-1.70	-1.71	-1.91	-1.660
07	ammonia-methane	C_{3v}	-0.54	-0.86	-0.86	-0.92	-0.771
08	methane-water	C_s	-0.54	-0.76	-0.76	-0.82	-0.665
09	formaldehyde dimer	C_s	-2.78	-3.82	-4.33	-5.23	-4.479
10	ethene-water	C_s	-2.11	-2.57	-2.59	-2.92	-2.564
11	ethene-formaldehyde	C_s	-1.32	-1.78	-1.73	-1.94	-1.623
12	ethyne dimer	C_{2v}	-1.28	-1.66	-1.59	-1.79	-1.529
13	ethene-ammonia	C_s	-1.05	-1.43	-1.44	-1.58	-1.382
14	ethene-dimer	C_{2v}	-0.71	-1.13	-1.15	-1.24	-1.106
15	methane-ethene	C_s	-0.34	-0.64	-0.61	-0.66	-0.509
	ME		0.43	-0.01	-0.05	-0.27	—
	MAE		0.43	0.14	0.08	0.27	—
	MA%E		25.2%	9.3%	7.2%	18%	—
	Dispersion-dominated bonds						
16	borane-methane	C_s	-0.57	-1.23	-1.39	-1.58	-1.513
17	methane-ethane	C_s	-0.58	-1.02	-1.00	-1.03	-0.836
18	methane-ethane	C_3	-0.44	-0.78	-0.75	-0.78	-0.614
19	methane-dimer	C_{3d}	-0.38	-0.53	-0.52	-0.52	-0.539
20	methane-Ar	C_{3v}	-0.32	-0.42	-0.41	-0.42	-0.405
21	ethene-Ar	C_{2v}	-0.27	-0.35	-0.35	-0.35	-0.365
22	ethene-ethyne	C_{2v}	+1.00	+1.04	+0.96	+1.15	+0.794
23	ethene dimer	D_{2h}	+1.11	+1.18	+1.09	+1.35	+0.909
24	ethyne dimer	D_{2h}	+1.30	+1.30	+1.20	+1.38	+1.084
	ME		0.26	0.08	0.03	0.08	—
	MAE		0.26	0.15	0.10	0.17	—
	MA%E		29.5%	17.4%	12.3%	20.1%	—

RPA correlation energy can be written as

$$\mathrm{Tr}\left\{v[\chi_\lambda^{\mathrm{RPA}}(iu) - \chi_s(iu)]\right\} = \sum_i \left[\frac{e_i(iu)}{1 - \lambda e_i(iu)} - e_i(iu)\right]. \quad (A2)$$

The integration over the coupling constant can be performed analytically and the final result for the RPA correlation energy becomes:

$$E_c^{\mathrm{RPA}} = \frac{1}{2\pi}\int_0^\infty du \sum_i \left[\ln[1 - e_i(iu)] + e_i(iu)\right]. \quad (A3)$$

The spectrum of the GEP in Eq. (A1) is bounded from above by zero, and only a small number of the lowest lying eigenvalues are significantly different from zero.[74,78] This implies that only a small fraction of the $\{e_i\}$ contributes significantly to the correlation energy, and an

efficient iterative diagonalization scheme can be used to evaluate those.[53,79] The basic operation involved in the iterative solution of the GEP in Eq. (A1) is the calculation of the noninteracting response to a trial potential, and this is done resorting to the linear-response techniques of density functional perturbation theory[76] (DFPT), generalized to imaginary frequencies.

2. The RPAx correlation energy

A strategy analogous to the one adopted for the RPA problem is used to compute the RPAx correlation energy. The GEP to solve in this case is the following

$$-\chi_s\left[v + f_x\right]\chi_s|z_\alpha^{\mathrm{RPAx}}\rangle = e_\alpha^{\mathrm{RPAx}}[-\chi_s]|z_\alpha^{\mathrm{RPAx}}\rangle. \quad (A4)$$

The expression for $\mathcal{H}_x = \chi_s f_x \chi_s$ in terms of KS orbitals and eigenvalues has been obtained by Görling,[80,81] and Hellgren and von Barth.[48] In this case the diagonalization was carried out in the basis set of the eigenvectors of the RPA GEP, Eq. (A1). This was done in order to i) avoid possible instabilities that may occur in the inversion of the non-interacting response function (i.e. the overlap matrix in the GEP) and ii) to speed up the calculations. On this basis set χ_s and $\mathcal{H}_H = \chi_s v \chi_s$ are diagonal and their matrix elements are readily available in terms of the eigenvalues of the RPA GEP (Eq. (A1)), i.e. $\chi_s^{ij} = \langle w_i | \chi_s | w_j \rangle = \delta_{ij} e_i$ and $\mathcal{H}_H^{ij} = \langle w_i | \chi_s v \chi_s | w_j \rangle = \delta_{ij} e_i^2$. The only additional operation required to solve the RPAx problem is the evaluation of the matrix elements $\mathcal{H}_x^{ij} = \langle w_i | \chi_s f_x \chi_s | w_j \rangle$. These can be efficiently computed using DFPT as detailed in Ref. 35 and 82. Once the solution of the GEP in Eq. (A4) is available the action of $v\chi_\lambda^{RPAx}$ on the eigenvectors $\{z_\alpha^{RPAx}\}$ can be explicitly expressed making use of the RPAx Dyson equation Eq. (23), i.e. $v\chi_\lambda^{RPAx}|z_\alpha^{RPAx}\rangle = v\chi_s|z_\alpha^{RPAx}\rangle/(1-\lambda e_\alpha^{RPAx})$, and the trace over spatial coordinates in the RPAx correlation energy can be written as

$$\mathrm{Tr}\left\{v[\chi_\lambda^{RPAx}(iu) - \chi_s(iu)]\right\} =$$
$$= \sum_\alpha \langle z_\alpha^{RPAx}|\chi_s v \chi_s|z_\alpha^{RPAx}\rangle_{iu}\left[1 - \frac{1}{1-\lambda e_\alpha^{RPAx}(iu)}\right]. \tag{A5}$$

The λ integration is analytic and the final result for the RPAx correlation energy reads

$$E_c^{RPAx} = -\frac{1}{2\pi}\int_0^\infty du \sum_\alpha \frac{\langle z_\alpha^{RPAx}|\chi_s v \chi_s|z_\alpha^{RPAx}\rangle_{iu}}{e_\alpha^{RPAx}(iu)}$$
$$\times \left[\ln[1 - e_\alpha^{RPAx}(iu)] + e_\alpha^{RPAx}(iu)\right] \tag{A6}$$

3. The RPAx(1) correlation energy

The RPAx(1) GEP is the following

$$vP_\lambda^{(1)}|z_{\lambda,\alpha}^{RPAx(1)}\rangle = e_{\lambda,\alpha}^{RPAx(1)}|z_{\lambda,\alpha}^{RPAx(1)}\rangle \tag{A7}$$

and it is solved in the basis set of the RPA eigenvectors [Eq. (A1)]. Also in this case the only additional information needed is the representation of the $\mathcal{H}_x$ operator on this basis (this may be already available if an RPAx calculation has been previously performed). The solution of the RPAx(1) GEP together with the RPAx(1) Dyson equation [Eq. (29)] allows to write explicitly $v\chi_\lambda^{RPAx(1)}|z_\alpha^{RPAx(1)}\rangle = e_{\lambda,\alpha}^{RPAx(1)}|z_\alpha^{RPAx(1)}\rangle/(1-\lambda e_{\lambda,\alpha}^{RPAx(1)})$, and the trace appearing in the correlation

energy expression becomes

$$\mathrm{Tr}\left\{v[\chi_\lambda^{RPAx(1)}(iu) - \chi_s(iu)]\right\} =$$
$$= \sum_\alpha \frac{e_{\lambda,\alpha}^{RPAx(1)}(iu)}{1-\lambda e_{\lambda,\alpha}^{RPAx(1)}(iu)} - \langle z_{\lambda,\alpha}^{RPAx(1)}|\chi_s|z_{\lambda,\alpha}^{RPAx(1)}\rangle_{iu} \tag{A8}$$

At variance with previous cases, for the RPAx(1) problem the integration over the coupling constant has to be performed numerically because of the non-trivial dependence of the eigenvalues and eigenvectors on coupling constant inherited from the λ-dependent GEP Eq. (A7). However the integrand is a smooth function and a Gauss-Legendre quadrature with less than five points ensures converged results within 0.01 kcal/mol (see Fig. 8). We stress here that the most computationally intensive part of the whole procedure is the evaluation of the response functions matrix elements. Once $\chi_s(iu)$ and $\mathcal{H}_{Hx}(iu)$ have been represented, only linear algebra operations with matrices of dimension $N_{eig} \times N_{eig}$ are needed to solve the GEP for each λ on the grids, meaning that the additional cost associated to the numerical coupling-constant integration is only a tiny fraction of the total computational cost.

4. The AC-SOSEX correlation energy

For the AC-SOSEX approximation the RPA eigenvectors $\{w_i\}$ from Eq. (A1) can be used to explicitly solve the SOSEX dyson equation [Eq. (31)] and compute the action of the SOSEX response function

$$v\chi_\lambda^{SOSEX}|w_i\rangle = \frac{(e_i + \lambda\mathcal{H}_x)|w_i\rangle}{1-\lambda e_i}. \tag{A9}$$
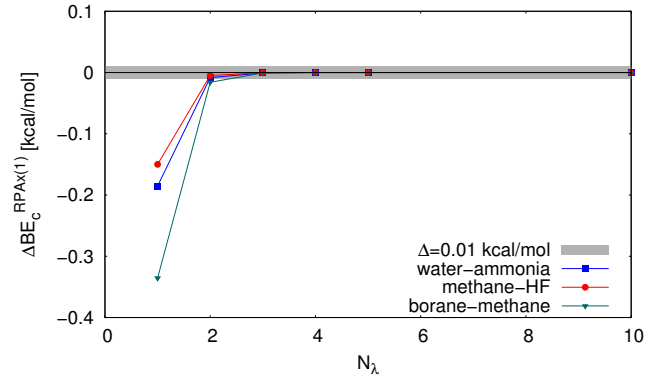

Figure 8. Convergence of the RPAx(1) binding energy with respect to the number of points in the λ grid for three different complexes.

The trace in the correlation energy expression can then be readily computed in the $\{|\omega_i\rangle\}$ basis set:

$$\text{Tr}\,\{v[\chi_\lambda^{\text{SOSEX}}(iu) - \chi_s(iu)]\} =$$
$$= \sum_i \frac{e_i(iu) + \lambda\mathcal{H}_{\text{x}}^{ii}(iu)}{1 - \lambda e_i(iu)} - e_i(iu). \qquad (A10)$$

The integration over the coupling constant is analytic and the final expression for the correlation energy reads

$$E_c^{\text{AC-SOSEX}} = \frac{1}{2\pi}\int_0^\infty du \sum_i \frac{e_i^2(iu) - \mathcal{H}_{\text{x}}^{ii}(iu)}{e_i^2}$$
$$\times [\ln(1 - e_i(iu)) + e_i] \qquad (A11)$$

[1] P. Hohenberg and W. Kohn, Phys. Rev. **136**, B864 (1964).

[2] W. Kohn and L. J. Sham, Phys. Rev. **140**, A1133 (1965).

[3] H. Hay, G. Ferlat, M. Casula, A. P. Seitsonen, and F. Mauri, Phys. Rev. B **92**, 144111 (2015).

[4] E. I. Román-Román and C. M. Zicovich-Wilson, Chemical Physics Letters **619**, 109 (2015).

[5] K. Rossnagel, Journal of Physics: Condensed Matter **23**, 213001 (2011).

[6] D. Varsano, S. Sorella, D. Sangalli, M. Barborini, S. Corni, E. Molinari, and M. Rontani, Nat. Comm. **8**, 1461 (2017).

[7] A. D. Becke, The Journal of Chemical Physics **98**, 1372 (1993).

[8] J. Heyd, G. E. Scuseria, and M. Ernzerhof, The Journal of Chemical Physics **118**, 8207 (2003).

[9] C. J. Cramer and D. G. Truhlar, Phys. Chem. Chem. Phys. **11**, 10757 (2009).

[10] L. Hedin, Phys. Rev. **139**, A796 (1965).

[11] P. García-González and R. W. Godby, Phys. Rev. Lett. **88**, 056406 (2002).

[12] N. Ferri, R. A. DiStasio, A. Ambrosetti, R. Car, and A. Tkatchenko, Phys. Rev. Lett. **114**, 176802 (2015).

[13] N. E. Dahlen and U. von Barth, Phys. Rev. B **69**, 195102 (2004).

[14] N. E. Dahlen, R. van Leeuwen, and U. von Barth, Phys. Rev. A **73**, 012511 (2006).

[15] M. Hellgren and U. von Barth, Phys. Rev. B **76**, 075107 (2007).

[16] D. L. Freeman, Phys. Rev. B **15**, 5512 (1977).

[17] A. Grüneis, M. Marsman, J. Harl, L. Schimka, and G. Kresse, The Journal of Chemical Physics **131**, 154115 (2009).

[18] X. Ren, P. Rinke, G. E. Scuseria, and M. Scheffler, Phys. Rev. B **88**, 035120 (2013).

[19] X. Ren, N. Marom, F. Caruso, M. Scheffler, and P. Rinke, Phys. Rev. B **92**, 081104 (2015).

[20] E. L. Shirley and R. M. Martin, Phys. Rev. B **47**, 15404 (1993).

[21] C. O. Almbladh, U. von Barth, and R. van Leeuwen, Int. J. Mod. Phys. B **13**, 535 (1999).

[22] G. Baym, Phys. Rev. **127**, 1391 (1962).

[23] G. Baym and L. P. Kadanoff, Phys. Rev. **124**, 287 (1961).

[24] E. Engel, in *A Primer in Density Functional Theory*, edited by C. F. et al. (Springer-Verlag Berlin Heidelberg, 2003).

[25] R. Del Sole, L. Reining, and R. W. Godby, Phys. Rev. B **49**, 8024 (1994).

[26] F. Bruneval, F. Sottile, V. Olevano, R. Del Sole, and L. Reining, Phys. Rev. Lett. **94**, 186402 (2005).

[27] P. Romaniello, S. Guyot, and L. Reining, The Journal of Chemical Physics **131**, 154111 (2009).

[28] H. Cao, Z. Yu, P. Lu, and L.-W. Wang, Phys. Rev. B **95**, 035139 (2017).

[29] J. Toulouse, I. C. Gerber, G. Jansen, A. Savin, and J. G. Ángyán, Phys. Rev. Lett. **102**, 096404 (2009).

[30] M. Hellgren and U. von Barth, J. Chem. Phys. **131**, 044110 (2009).

[31] A. Heßelmann and A. Görling, Molecular Physics **108**, 359 (2010).

[32] M. Hellgren and U. von Barth, J. Chem. Phys. **132**, 044101 (2010).

[33] A. Hesselmann and A. Görling, Phys. Rev. Lett. **106**, 093001 (2011).

[34] J. E. Bates and F. Furche, The Journal of Chemical Physics **139**, 171103 (2013).

[35] N. Colonna, M. Hellgren, and S. de Gironcoli, Phys. Rev. B **90**, 125150 (2014).

[36] A. Dixit, J. G. Ángyán, and D. Rocca, The Journal of Chemical Physics **145**, 104105 (2016).

[37] B. Mussard, D. Rocca, G. Jansen, and J. G. Ángyán, J. Chem. Theory Comput. **12**, 2191 (2016).

[38] A. Dixit, J. Claudot, S. Lebègue, and D. Rocca, Journal of Chemical Theory and Computation **13**, 5432 (2017).

[39] J. E. Bates, J. Sensenig, and A. Ruzsinszky, Phys. Rev. B **95**, 195158 (2017).

[40] J. Řezáč and P. Hobza, J. Chem. Theory Comput. **9**, 2151 (2013).

[41] A. L. Fetter and J. D. Walecka, *Quantum Theory of Many-Particle Systems* (Dover Publications, 2003).

[42] D. Langreth and J. Perdew, Solid State Commun. **17**, 1425 (1975).

[43] E. Runge and E. K. Gross, Phys. Rev. Lett **52**, 997 (1984).

[44] M. Hellgren, Eur. Phys. J. B **91**, 155 (2018).

[45] F. Caruso, D. R. Rohr, M. Hellgren, X. Ren, P. Rinke, A. Rubio, and M. Scheffler, Physical Review Letters **110**, 146403 (2013).

[46] M. Hellgren, F. Caruso, D. R. Rohr, X. Ren, A. Rubio, M. Scheffler, and P. Rinke, Physical Review B **91**, 165110 (2015).

[47] L. Sham and M. Schlüter, Phys Rev B **32**, 3883 (1985).

[48] M. Hellgren and U. von Barth, Phys. Rev. B **78**, 115107 (2008).

[49] Y.-H. Kim and A. Görling, Phys. Rev. B **66**, 035114 (2002).

[50] W. Zhu, J. Toulouse, A. Savin, and J. G. Ángyán, The Journal of Chemical Physics **132**, 244108 (2010).

[51] N. Colonna, M. Hellgren, and S. de Gironcoli, Phys. Rev. B **93**, 195108 (2016).

[52] P. Giannozzi, O. Andreussi, T. Brumme, O. Bunau, M. B. Nardelli, M. Calandra, R. Car, C. Cavazzoni, D. Ceresoli, M. Cococcioni, N. Colonna, I. Carnimeo, A. D. Corso, S. de Gironcoli, P. Delugas, R. A. D. Jr, A. Ferretti, A. Floris, G. Fratesi, G. Fugallo, R. Gebauer, U. Gerst-

mann, F. Giustino, T. Gorni, J. Jia, M. Kawamura, H.-Y. Ko, A. Kokalj, E. E. K. cúkbenli, M. Lazzeri, M. Marsili, N. Marzari, F. Mauri, N. L. Nguyen, H.-V. Nguyen, A. O. de-la Roza, L. Paulatto, S. Poncé, D. Rocca, R. Sabatini, B. Santra, M. Schlipf, A. P. Seitsonen, A. Smogunov, I. Timrov, T. Thonhauser, P. Umari, N. Vast, X. Wu, and S. Baroni, Journal of Physics: Condensed Matter **29**, 465901 (2017).

[53] H.-V. Nguyen and S. de Gironcoli, Phys. Rev. B **79**, 205114 (2009).

[54] N. L. Nguyen, N. Colonna, and S. de Gironcoli, Phys. Rev. B **90**, 045138 (2014).

[55] W. Kolos and L. Wolniewics, J. Chem. Phys. **43**, 2429 (1965).

[56] X. Ren, P. Rinke, C. Joas, and M. Scheffler, Journal of Materials Science **47**, 7447 (2012).

[57] T. Olsen and K. S. Thygesen, The Journal of Chemical Physics **140**, 164116 (2014).

[58] M. Fuchs, Y.-M. Niquet, X. Gonze, and K. Burke, The Journal of Chemical Physics **122**, 094116 (2005).

[59] T. M. Henderson and G. E. Scuseria, Molecular Physics **108**, 2511 (2010).

[60] D. M. Ceperley and B. J. Alder, Phys. Rev. Lett. **45**, 566 (1980).

[61] S. Moroni, D. M. Ceperley, and G. Senatore, Phys. Rev. Lett. **75**, 689 (1995).

[62] E. Maggio and G. Kresse, Phys. Rev. B **93**, 235113 (2016).

[63] J. Toulouse, W. Zhu, A. Savin, G. Jansen, and J. G. Ángyán, The Journal of Chemical Physics **135**, 084119 (2011).

[64] J. Erhard, P. Bleiziffer, and A. Görling, Phys. Rev. Lett. **117**, 143002 (2016).

[65] P. Giannozzi, S. Baroni, N. Bonini, M. Calandra, R. Car, C. Cavazzoni, D. Ceresoli, G. L. Chiarotti, M. Cococcioni, I. Dabo, A. D. Corso, S. d. Gironcoli, S. Fabris, G. Fratesi, R. Gebauer, U. Gerstmann, C. Gougoussis, A. Kokalj, M. Lazzeri, L. Martin-Samos, N. Marzari, F. Mauri, R. Mazzarello, S. Paolini, A. Pasquarello, L. Paulatto, C. Sbraccia, S. Scandolo, G. Sclauzero, A. P. Seitsonen, A. Smogunov, P. Umari, and R. M. Wentzcovitch, J. Phys.: Condens. Matter **21**, 395502 (2009).

[66] J. P. Perdew, K. Burke, and M. Ernzerhof, Phys. Rev. Lett. **77**, 3865 (1996).

[67] D. R. Hamann, Phys. Rev. B **88**, 085117 (2013).

[68] M. Schlipf and F. Gygi, Computer Physics Communications **196**, 36 (2015).

[69] "SG15 ONCV Potentials," (2017).

[70] F. Gygi and A. Baldereschi, Phys. Rev. B **34**, 4405 (1986).

[71] J. Spencer and A. Alavi, Phys. Rev. B **77**, 193110 (2008).

[72] M. Marsili and P. Umari, Phys. Rev. B **87**, 205110 (2013).

[73] D. Lu, Y. Li, D. Rocca, and G. Galli, Phys. Rev. Lett. **102**, 206411 (2009).

[74] H. F. Wilson, F. Gygi, and G. Galli, Phys. Rev. B **78**, 113303 (2008).

[75] D. Rocca, The Journal of Chemical Physics **140**, 18A501 (2013).

[76] S. Baroni, S. de Gironcoli, A. Dal Corso, and P. Giannozzi, Rev. Mod. Phys. **73**, 515 (2001).

[77] This can be done since that the density–density response functions are analytic in the upper half-plane and vanish at infinity faster than ω^{-1} (see for instance Ref. **?**).

[78] A. Baldereschi and E. Tosatti, Solid State Communications **29**, 131 (1979).

[79] H.-V. Nguyen, *Efficient calculation of RPA correlation energies in the Adiabatic-Connection Fluctuation-Dissipation theory*, Ph.D. thesis, Internatinal School for Advanced Studies (SISSA) (2008).

[80] A. Görling, Phys. Rev. A **57**, 3433 (1998).

[81] A. Görling, Int. J. Quantum Chem. **69**, 265 (1998).

[82] N. Colonna, *Exchange and Correlation Energy in the Adiabatic Connection Fluctuation-Dissipation theory beyond RPA*, Ph.D. thesis, Internatinal School for Advanced Studies (SISSA) (2014).